Geophys. J. Int. (2004) **159,** 749–764 doi: 10.1111/j.1365-246X.2004.02425.x

Crustal structure of the Peruvian continental margin from wide-angle seismic studies

A. Krabbenhöft,[1] J. Bialas,[1] H. Kopp,[1] N. Kukowski[2] and C. Hübscher[3]

[1] *Leibniz Institute of Marine Sciences (IFM-GEOMAR), Wischhofstrasse* 1-3, 24148 *Kiel, Germany. E-mails: akrabbenhoeft@ifm-geomar.de (AK); jbialas@ifm-geomar.de (JB); hkopp@ifm-geomar.de (HK)*

[2] *GeoForschungsZentrum Potsdam, Telegrafenberg,* 14473 *Potsdam, Germany. E-mail: nina@gfz-potsdam.de*

[3] *Center for Marine and Climate Research, Institute for Geophysics, University of Hamburg, Bundesstrasse* 55, 20146 *Hamburg, Germany. E-mail: huebscher@dkrz.de*

Accepted 2004 July 15. Received 2004 June 24; in original form 2003 October 21

SUMMARY

Active seismic investigations along the Pacific margin off Peru were carried out using ocean bottom hydrophones and seismometers. The structure and the *P*-wave velocities of the obliquely subducting oceanic Nazca Plate and overriding South American Plate from 8°S to 15°S were determined by modelling the wide-angle seismic data combined with the analysis of reflection seismic data. Three detailed cross-sections of the subduction zone of the Peruvian margin and one strike-line across the Lima Basin are presented here.

The oceanic crust of the Nazca Plate, with a thin pelagic sediment cover, ranging from 0–200 m, has an average thickness of 6.4 km. At 8°S it thins to 4 km in the area of Trujillo Trough, a graben-like structure. Across the margin, the plate boundary can be traced to 25 km depth. As inferred from the velocity models, a frontal prism exists adjacent to the trench axis and is associated with the steep lower slope. Terrigeneous sediments are proposed to be transported downslope due to gravitational forces and comprise the frontal prism, characterized by low seismic *P*-wave velocities. The lower slope material accretes against a backstop structure, which is defined by higher seismic *P*-wave velocities, 3.5–6.0 km s^{-1}. The large variations in surface slope along one transect may reflect basal removal of upper plate material, thus steepening the slope surface. Subduction processes along the Peruvian margin are dominated by tectonic erosion indicated by the large margin taper, the shape and bending of the subducting slab, laterally varying slope angles and the material properties of the overriding continental plate. The erosional mechanisms, frontal and basal erosion, result in the steepening of the slope and consequent slope failure.

Key words: continental margin, forward model, Peru, subduction zone, velocity model, wide-angle seismic data.

1 INTRODUCTION

In the late 1970s extensive geological and geophysical studies were carried out along the continental margin of Peru within the Nazca Plate Project (Kulm *et al.* 1981). In 1988 ten sites on the Peruvian margin were drilled during Ocean Drilling Program (ODP) Leg 112 and correlated with high-quality seismic multichannel (MCS) data (line CDP-1), acquired in 1972 at 12°S by the Shell Oil Co. (von Huene & Suess 1988). These lines were later depth migrated and used along with MCS data acquired by the Hawaii Institute of Geophysics (Moore & Taylor 1988) to re-evaluate the tectonic processes across the Peru margin (von Huene *et al.* 1996). These studies only partly cover the Peruvian margin—mainly the northern area, where the uplift and subsidence history, due to the passing Nazca Ridge, was investigated, as well as the resulting tectonic processes and the material transfer modes, i.e. the erosional effects of Nazca Ridge subduction.

Seismic reflection and refraction data were acquired during the R/V *Sonne* cruise SO146 offshore of Peru in 2000 (Bialas & Kukowski 2000). The seismic data were supplemented by high-resolution bathymetry and gravity data. Heat flow measurements were conducted along with seafloor sampling and video observations (Pecher *et al.* 2001). Quantitative characterization of the structures and geodynamics of the Peruvian section of the Andean subduction zone and the associated gas hydrate systems in regions with variable tectonic histories were the main objectives of this cruise. Integrating the geological and geophysical information mentioned above, this study concentrates on the analysis of four wide-angle seismic profiles acquired across and along the margin during cruise SO146. The aim is to obtain the deep crustal structure and

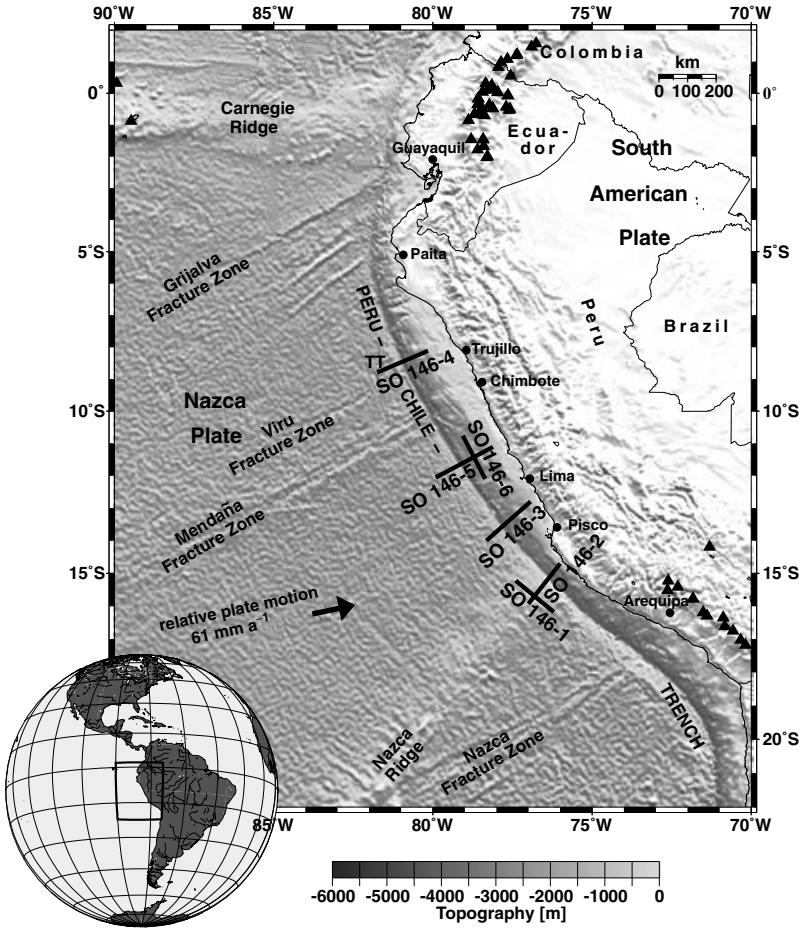

Figure 1. Geodynamic setting of the Peruvian continental margin. Bathymetry is taken from Sandwell & Smith (1997) and illumination is from the northeast. Norabuena *et al.* (1999) determined the plate motion vector. The Mendaña Fracture Zone (MFZ) divides the study area into a northern and southern province of different oceanic crustal age. The Trujillo Trough connects the Viru Fracture Zone, which parallels the MFZ, with the trench. The active volcanic arc is marked by triangles (taken from the Smithsonian Institution catalogue, available at http://www.volcano.si.edu/world/summinfo.cfm).

derive tectonic processes from the velocity models along the entire Peruvian margin. The high-resolution MCS data acquired earlier (von Huene & Suess 1988), mentioned above, helped improve the first kilometres of the velocity–depth models, and therefore the resolution of the entire crustal structure at 12°S.

Oblique subduction of the Nazca Pate and the resulting southward migration of the Nazca Ridge along the margin characterizes the region investigated during cruise SO146 (Fig. 1). It was believed that the entire Peruvian margin, starting at 5°S to the present collision zone at 15°S, was affected by Nazca Ridge subduction (von Huene *et al.* 1996). A re-evaluation of the migration history of the Nazca Ridge, using updated plate motion data, yields the northernmost collision zone of the Nazca Ridge with the South American Plate at 11°S (Hampel 2002). Thus, three of the seismic profiles, SO146-5 and SO146-6, both at 12°S, and SO146-3 at 14°S (Fig. 2), cover the area where the subducting Nazca Ridge has passed during the last 11 Myr (Hampel 2002), in order to study the subduction processes at different stages after Nazca Ridge subduction. They represent 'time slices' and thus allow the process of 'returning to equilibrium' in the wake of the ridge crest subduction to be reconstructed (von Huene *et al.* 1996). The northernmost profile (SO146-4/9°S) characterizes portions of the Peruvian margin which have not been affected by ridge subduction (Hampel 2002). Therefore, we assume that this part of the Peruvian margin represents the 'state of equilibrium', and take profile SO146-4/9°S as a reference to compare with the lines affected by Nazca Ridge subduction.

2 STUDY AREA

The oceanic Nazca Plate originates from the fast-spreading East Pacific Rise, whose full spreading rate is 150 mm yr^{-1} (Purdy *et al.* 1992). The plate is moving largely eastwards (N78°E) with a velocity of about 61 mm Myr^{-1}, resulting in convergence oblique to the trench as it bends to the southeast (Norabuena *et al.* 1999). The Peru–Chile Trench, with water depths of more than 6000 m, is where the Nazca Plate is subducting underneath the continental South American Plate (Fig. 1). The Nazca Plate is segmented by fracture zones, leading to different crustal ages along the plate boundary. The Mendaña Fracture Zone trends N65°E and marks a transition zone of a crustal age difference of about 10 Myr, as revealed by magnetic anomalies (Hussong *et al.* 1984). Consequently, at the trench, the Nazca Plate is about 38 Myr old off central and south Peru and about 28 Myr old north of the Mendaña Fracture Zone (Müller *et al.* 1997). The increasing age of the oceanic crust of the southern segment coincides with the increasing water depth from 4500 m in the north to 5000 m south of the Mendaña Fracture Zone (Hilde & Warsi 1982). The Viru Fracture Zone parallels the Mendaña Fracture Zone 110 km further north and joins the Trujillo

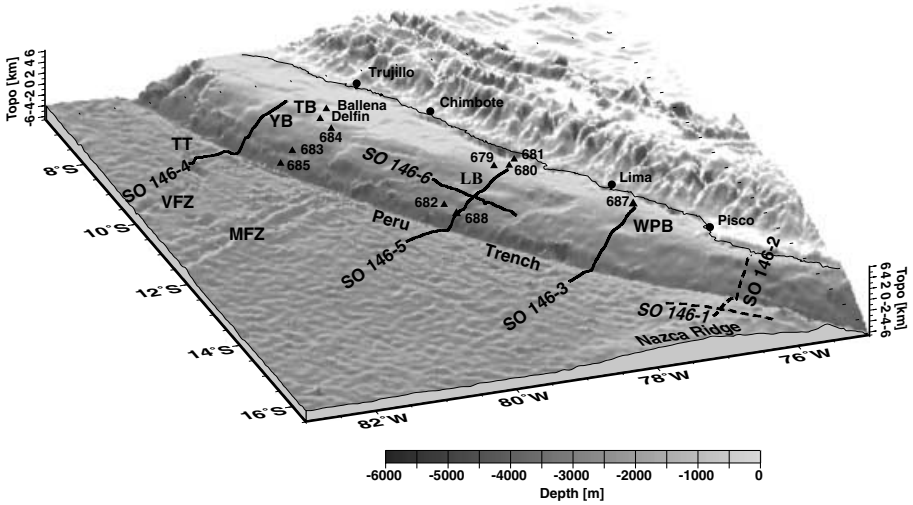

Figure 2. A detailed overview of the GEOPECO study area with bathymetry data from Sandwell & Smith (1997); illumination is from the northeast. The solid lines are the positions of the GEOPECO wide-angle seismic profiles discussed within this study, whereas the dashed lines are the positions of the GEOPECO wide-angle seismic profiles presented by Hampel *et al.* (2004). Profile SO146-4/9°S covers the Trujillo Trough (TT) at its seawardmost part. Annotated triangles mark the drill sites. LB, Lima Basin; MFZ, Mendaña Fracture Zone; TB, Trujillo Basin; VFZ, Viru Fracture Zone; WPB, West Pisco Basin; YB, Yaquina Basin.

Trough, a reverse fault, which is trending N15°E, connecting the Viru Fracture Zone with the Peru–Chile Trench (Huchon & Bourgois 1990) (Figs 1 and 2). The oceanic plate east of the Trujillo Trough is characterized by a rough fabric trending perpendicular to the Mendaña Fracture Zone (Huchon & Bourgois 1990).

The study area is bounded by two aseismic bathymetric highs (Fig. 1). Carnegie Ridge in the north originates from the Galapagos hotspot (Collot *et al.* 2002). Nazca Ridge in the south was formed at a melting anomaly in the Pacific–Farallon/Nazca spreading centre, simultaneously with the aseismic Tuamoto Ridge, its mirror image on the Pacific Plate in the west (Pilger & Handschumacher 1981; Ito *et al.* 1995). Four forearc basins (extension is indicated by normal faulting (von Huene *et al.* 1996)) are located on the forearc in the study area from north to south: Trujillo and Yaquina basins at 9°S, Lima Basin at 11°S and West Pisco Basin at 13°S (Fig. 2). The latter two were affected by the southward migration of the Nazca Ridge, which caused uplift and subsidence along the margin leading to increased rates of erosion (von Huene & Suess 1988; Pecher *et al.* 1996; Clift *et al.* 2003). The coastline of Peru is also affected by the Nazca Ridge, forming a seaward bulge where it is currently subducting. An eastward migration of the continental margin north of Peru since the Mesozoic is linked to subduction erosion (von Huene & Scholl 1991). An eastward shift from the position of the Mesozoic magmatic arc to the Late Cenozoic arc is also documented in Peru (McKee & Noble 1990) consistent with net erosion. The buoyancy of the thickened oceanic crust of the Nazca Ridge is associated with flat subduction (Vogt *et al.* 1976; Pilger 1981; Norabuena *et al.* 1994) and uplift of the continental upper plate. Flat subduction is coincident with the lack of Quaternary volcanism (Fig. 1) as observed in other places where ridge subduction is occurring, e.g. the Cocos Ridge underneath Costa Rica and the Juan Fernandez Seamount Chain underneath Chile (Pilger 1981; Protti *et al.* 1995; Gutscher *et al.* 2000).

3 SEISMIC DATA

3.1 Wide-angle data

Seismic measurements off Peru were carried out using the R/V *Sonne* during cruise SO146 (Bialas & Kukowski 2000). Six wide-angle seismic profiles were shot with an array of three 32-l airguns at a shot interval of 60 s and a ship speed of 4 knots, resulting in an average shot spacing of 120 m. Data were recorded by a total of 97 stations using GEOMAR ocean bottom hydrophones (OBH) (Flueh & Bialas 1996) and seismometers (OBS) (Bialas & Flueh 1999).

3.2 Processing procedure

The refraction seismic data were corrected with relocated OBH/S positions. The seismic signal holds frequencies from 4 to 16 Hz for the different phases. A time- and offset-dependent frequency filter was applied to adjust for the time- and offset-dependent variations. To further improve the temporal resolution of the seismic data, a gated Wiener deconvolution was applied to compress the basic seismic wavelet. Data quality is very good and the source energy was sufficient to receive signals from a distance of at least 130 km from the OBH/S stations, penetrating to a depth of about 30 km. Station OBH 43 of profile SO146-4 (Fig. 3) is a representative example of the seismic sections.

3.3 Reflection data

Multichannel seismic (MCS) data were acquired simultaneously with the refraction profiles (Figs 4 and 5). A 24-channel streamer recorded the seismic signal along an active length of 150 m and was towed about 50 m behind the ship's stern (Bialas & Kukowski 2000). The data were sorted for common midpoints and a frequency filter was applied before stacking. Due to the low-frequency content of the seismic signal and the great water depth across the lower slope the Fresnel zone is large. Spatial aliasing occurs at steep topographic features as a consequence of the 150 m shot point distance. Hence, structures beneath the steep lower slope, such as the frontal prism, cannot be resolved.

4 MODELLING

To obtain the deep structure of the margin and the *P*-wave velocity field, a forward modelling technique was performed on profiles SO146-3/14°S, SO146-4/9°S and SO146-5/12°S (Figs 6–9). With

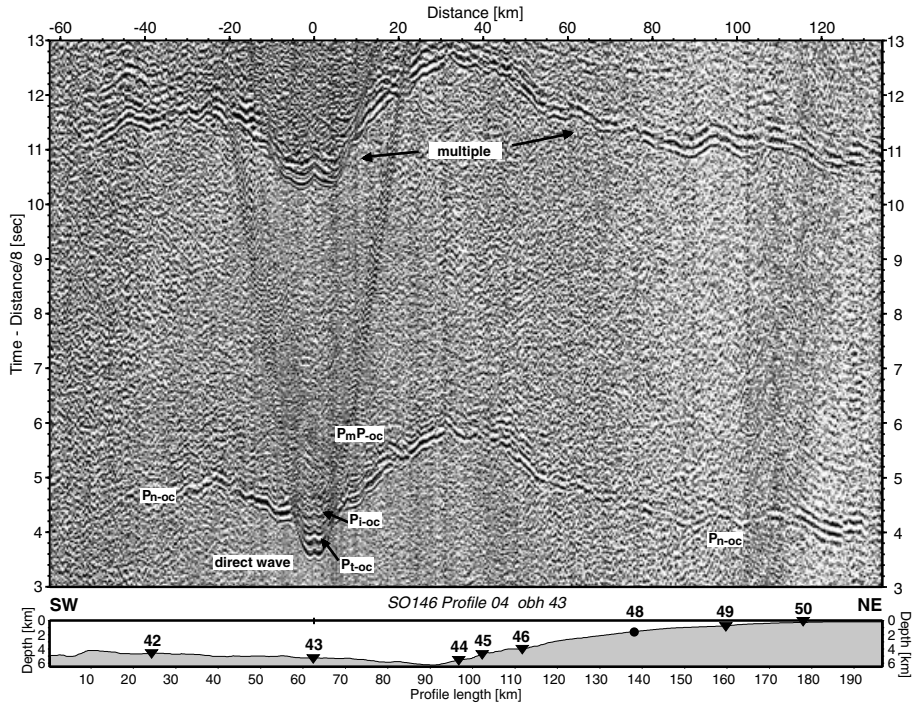

Figure 3. Representative example of a wide-angle seismic section recorded by OBH 43 located on the oceanic crust on the northernmost profile SO146-4/9°S. The data are displayed with a reduction velocity of 8 km s^{-1}. $P_{t\text{-}oc}$ and $P_{i\text{-}oc}$ denote the reflections from the top of the oceanic crust and from the intracrustal boundary, respectively. The mantle refraction P_n shows a good signal as far as 130 km offset from the OBH position. P_mP denotes the reflected wave from the crust–mantle boundary. The topography along the profile is shown underneath the seismic section with all the locations of the OBH/S stations, triangles and circles mark OBH and OBS stations, respectively.

this technique not only the first arrivals but also later refraction and reflection phases could be used to resolve complicated structures on the profiles. A tomographic inversion was applied on strike-line SO146-6/12°S. The starting models for both methods include the known bathymetry. The resulting models of the combined analysis of the reflection and refraction seismic data are shown in Figs 10 and 11. The major horizons (top of oceanic crust, subducting slab, top of the crystalline basement (top of Eocene; Fig. 4b)) identified in the MCS sections are correlated with the reflection phases from the wide-angle data at zero offset (Fig. 5) to provide a starting model for forward modelling (Luetgert 1992; Zelt 1999).

The reflection and refraction arrivals were identified and picked on all seismic OBH/S sections. Picking accuracy in the seismogram sections is better than 50 ms for the near offset range (i.e. ±100 m with a velocity of 2 km s^{-1}), as well as for oceanic crustal phases, and is better than 100 ms for large offsets (i.e. ±500 m with a velocity of 5 km s^{-1}) where seismic phases interfere with strong multiple reverberations of the direct wave from previous shots. Due to reverberations resulting from the shallow water depth on the upper slope and shelf region, picking accuracy decreases in this area for the near offset range on all dip lines. The top of the subducting oceanic plate (designated $P_{t\text{-}oc}$; Figs 3 and 6–9) is well identified on all profiles up to a distance of 60 km landwards of the trench. On all three dip lines north of Nazca Ridge, a reflection from an intracrustal reflector within the subducting oceanic plate (designated $P_{i\text{-}oc}$; Figs 6, 8 and 9) is clearly visible. The change in gradient of the first arrival at a distance of around ±10 km from the OBH position (refraction from upper crustal layer, $P_{u\text{-}oc}$, to the refraction of the lower crustal layer, $P_{l\text{-}oc}$; enlargement of OBH station 51, Fig. 6) additionally supports the existence of the intracrustal oceanic boundary across the Peruvian margin. $P_mP_{\text{-}oc}$ is the mantle reflection within the subducting oceanic plate with its corresponding refraction $P_{n\text{-}oc}$ (Figs 3 and 6–9).

4.1 Forward modelling

A 2-D seismic ray tracing method was applied using the MacRay program (Luetgert 1992). Calculated traveltimes from the velocity model are compared with the seismic refraction datasets. Examples are given for each profile in Figs 7–9. The strong multiple arrivals observed in some OBH/S stations were used to identify seismic events, e.g. $P_{n\text{-}oc}$ of the downgoing slab on SO146-4/9°S OBH 44 (Fig. 7). The modelled data fit the wide-angle data very well, with mean traveltime deviations being within the picking accuracy.

4.2 Tomography

Line SO146-6/12°S runs perpendicular to profile SO146-5/12°S, with a denser OBH/S spacing of about 10 km. This geometry allows a tomographic inversion on this profile to derive the *P*-velocity structure underneath the Lima Basin (Fig. 11) using the First Arrival Seismic Tomography (FAST) code (Zelt & Barton 1998). The velocity distribution obtained along line SO146-5/12°S by forward modelling at the junction with profile SO146-6 served as a starting model. Only the first arrivals of the seismic records were picked and used for the traveltime inversion. First arrivals were generally picked within an accuracy of 30 ms for the near-offset range and 80 ms for far offsets. Picking uncertainty is no more than 120 ms for phases where identification was not clearly distinct. A coverage of up to 2000 hits per cell was achieved, which yields good resolution of the crustal structure and the boundary between the continental and the subducting oceanic plate, with only some restrictions in the peripheral region of the model (Fig. 11).

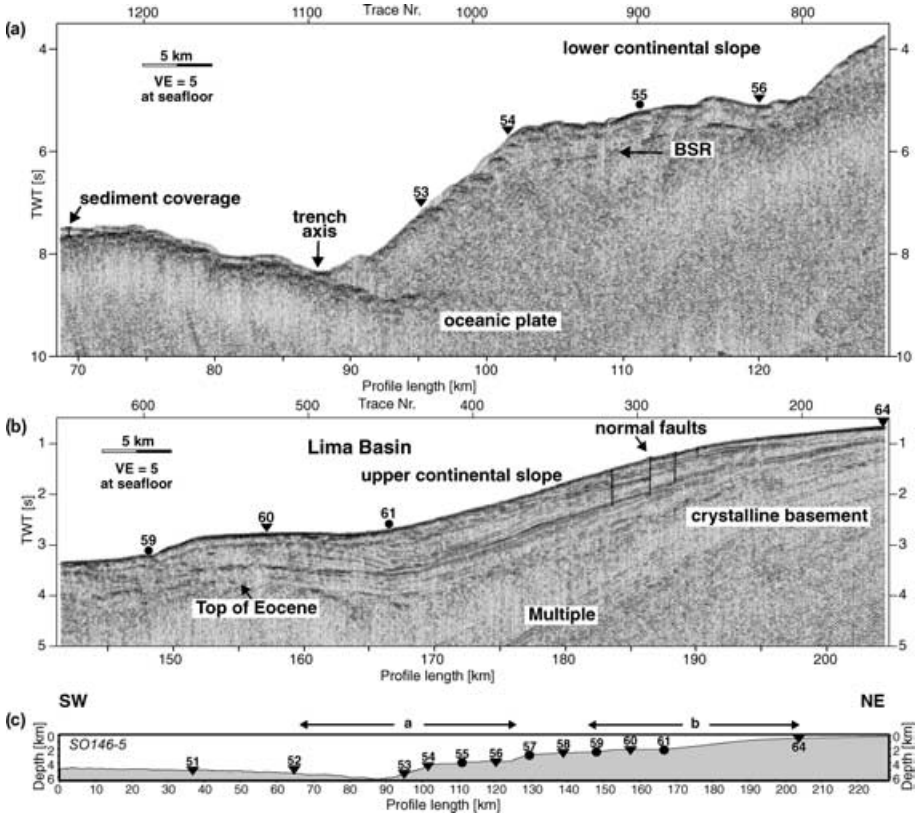

Figure 4. Two parts of reflection seismograms from profile SO146-5/12°S are displayed. The locations of the OBH and OBS stations are marked with triangles and circles, respectively. The subducting oceanic plate with a thin pelagic sediment layer can be traced up to 15 km from the trench axis (a). A prominent BSR is present underneath the lower slope. The landward part of the seismic section (b) reveals erosional tectonic features. Extension is indicated by normal faulting. The interpretation of the horizons follows von Huene & Suess (1988) and von Huene *et al.* (1996). Vertical exaggeration at seafloor is $VE = 5$. (c) The topography of line SO146-5/12°S and locations of OBH/S stations for orientation.

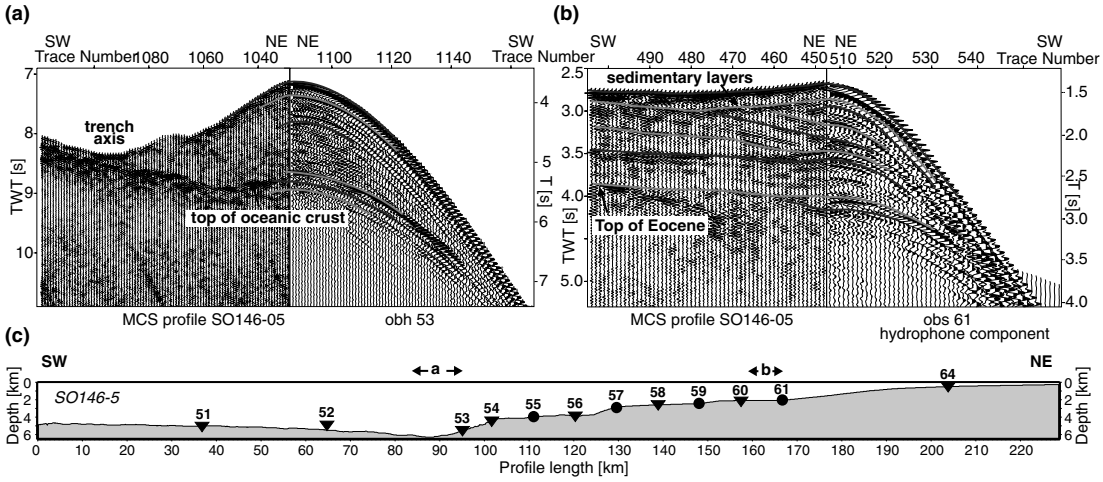

Figure 5. Reflection seismograms in the left parts of the figures and OBH/S stations in the right parts of the figures. This type of display supports the identification and correlation of reflection seismic events between MCS and wide-angle seismic data in order to support forward modelling. (a) The subducting slab underneath the continental margin, which can be correlated with the $P_{t\text{-}oc}$ phase denoting the reflection from the top of the oceanic crust. The OBH station in this figure (b) is located at the upper slope of the continental margin. Several sedimentary phases can be identified in both seismic sections as well as the top of the crystalline basement. (c) The topography of profile SO146-5/12°S and locations of OBH/S stations for orientation.

5 RESULTS

5.1 Reflection data

MCS line SO146-5/12°S in Fig. 4(a) shows the typical sediment thickness of the oceanic crust offshore Peru, with ∼150 m around profile km 70 and ∼0 m around profile km 75. The subducting slab is traced up to 15 km landwards of the deformation front. A bottom-simulating reflector (BSR) on the lower slope indicates the presence of gas hydrates, marking the base of the gas hydrate stability zone. Across the Lima Basin several sediment sequences reveal the erosional and transgressional history of the upper slope and onlap onto

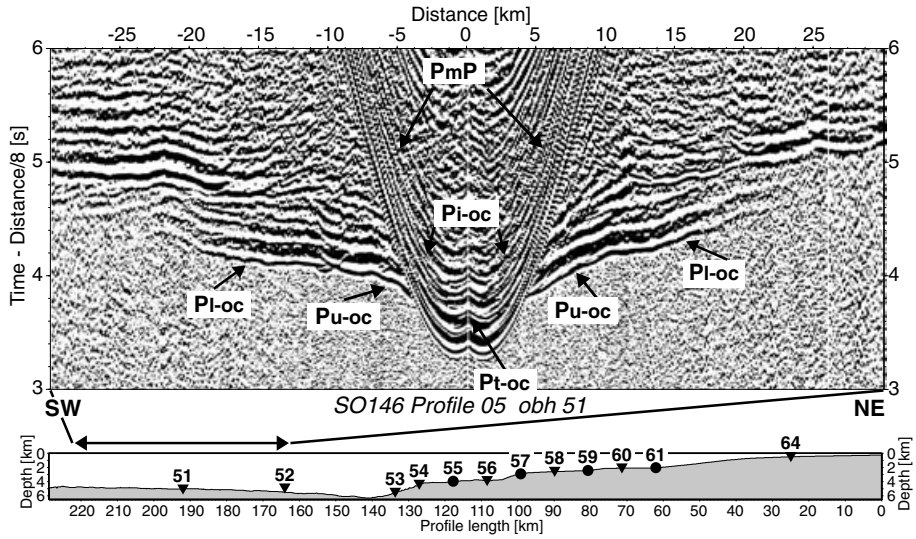

Figure 6. Near-offset traces of the wide-angle seismic section recorded by OBH 51 located on the oceanic crust on profile SO146-5/12°S. The data are displayed with a reduction velocity of 8 km s^{-1}. $P_{t\text{-}oc}$, $P_{i\text{-}oc}$ and P_mP are reflections from the top of the oceanic crust, the intracrustal boundary and the crust–mantle boundary. $P_{u\text{-}oc}$ and $P_{l\text{-}oc}$ are refractions from the upper oceanic crust and the lower oceanic crust. The topography along the entire profile is shown underneath the seismic section with all the locations of the OBH/S stations; triangles and circles mark OBH and OBS stations, respectively.

the Peru shelf (Pecher *et al.* 2001; Clift *et al.* 2003). The thick diffracting section beneath the continental margin marks the top of the crystalline basement. Additional high-resolution MCS data from line CDP-1, published by von Huene & Suess (1988), were used to relate the geological structures to the seismic velocities, obtained by forward modelling, especially along the lower and middle slope. The MCS line drawing (von Huene & Suess 1988) of line CDP-1 correlated with the coincident time-converted refraction model of profile SO146-5/12°S is shown in Fig. 12.

5.2 The oceanic plate

The Nazca Plate shows an overall rough topography, as revealed by satellite-derived predicted bathymetry (Figs 1 and 2) and detailed swath bathymetry published by Kukowski *et al.* (2002). This is also apparent in the wide-angle seismic data, e.g. the undulations of the refracted phase that travelled through the mantle. It is denoted as $P_{n\text{-}oc}$ at the westernmost part of the model originating from Trujillo Trough in Figs 7(b) and (d). There are differences in the oceanic crust north and south of the Mendaña Fracture Zone, which are discussed below.

The Trujillo Trough is located on the westernmost part of profile SO146-4/9°S (Fig. 2) and is characterized by a graben-like structure, which is 5 km wide with a vertical offset of about 500 m at the seafloor. This graben-like structure is also extending into the igneous crust (Fig. 10a). Modelled traveltime curves of this line compared with the seismic refraction dataset, e.g. OBH 42 in Fig. 13, are consistent with the downward continuation of Trujillo Trough to the Moho, 4 km below the seafloor. Gravity modelling (Heinbockel *et al.* 2003) supports the results obtained from the refraction seismic data of the oceanic crustal structure in this region. Immediately east of the Trujillo Trough the crust is elevated about 1-km relative to that west of the trough, as far as profile km 35. This elevation is concurrent with a very thin sediment layer and a relatively thin oceanic crust of about 4 km thickness (Figs 10a, 13). The model is consistent with the arrivals of the Moho reflection occurring ∼1.7 s two-way traveltime (TWT) after the direct arrival at OBH station 42, and ∼2.1 s TWT at OBH station 43 ($P_mP_{\text{-}oc}$, Fig. 13), with 'normal' oceanic crustal thickness. This 30 km long segment of thinned oceanic crust (Fig. 10a) is linked to the east–west extensional regime proposed by Huchon & Bourgois (1990). The topographic highs and lows trending perpendicular to the Mendaña Fracture Zone and which are located eastwards of the Trujillo Trough in the vicinity of OBH 43 persist downwards at least to the intracrustal oceanic boundary (Figs 2 and 10).

The oceanic crust south of the Mendaña Fracture Zone differs from the structures observed in profile SO146-4/9°S. The ocean floor shows a rough topography, but without specific orientation and in contrast to the northern line (SO146-4/9°S). This rough topography along profiles SO146-5/12°S and SO146-3/14°S extends only to the upper crustal boundary but not to the Moho. The velocity model of profile SO146-5/12°S (Fig. 10b) is consistent with a very thin sedimentary layer, locally with a maximum thickness of about 200 m. The rough oceanic basement sporadically outcrops, e.g. between profile length 20–30 km. The sedimentary cover throughout the southern profile SO146-3/14°S (Fig. 10c) is slightly thicker because there is no outcropping ocean crust, but the maximum sediment thickness is also 200 m. The oceanic crustal layers of these two seismic models are similar overall. Comparing the crustal thicknesses of profiles SO146-5/12°S and SO146-3/14°S, there is an increase of ∼0.5 km towards the south, which we suggest as reflecting the outermost edge of the Nazca Ridge.

The crustal structure of the Nazca Plate was determined from the reflected P waves at the top of the oceanic crust $P_{t\text{-}oc}$, the intracrustal reflection $P_{i\text{-}oc}$ and the reflection from the crust–mantle interface P_mP. The refracted waves travelling through the upper crustal layers $P_{u\text{-}oc}$ are consistent with velocities gradually increasing from 4.7–6.1 km s^{-1} and the refractions of the lower crustal layer $P_{l\text{-}oc}$ with velocities from 6.4–7.3 km s^{-1} with some small regional variations (see the traveltime curves in Figs 7–9 and 13). The oceanic crust has a mean total thickness of 6.4 km resulting from a 1.6–2.1 km thick upper crustal layer and a lower crust with a thickness of 4.2–5.2 km (Fig. 10). The position of the Moho and the velocity distribution in the mantle were derived from the P waves reflected (at pre- and post-critical angle) at the crust–mantle interface P_mP and the corresponding refraction P_n (Figs 7b–9b and 7c–9c).

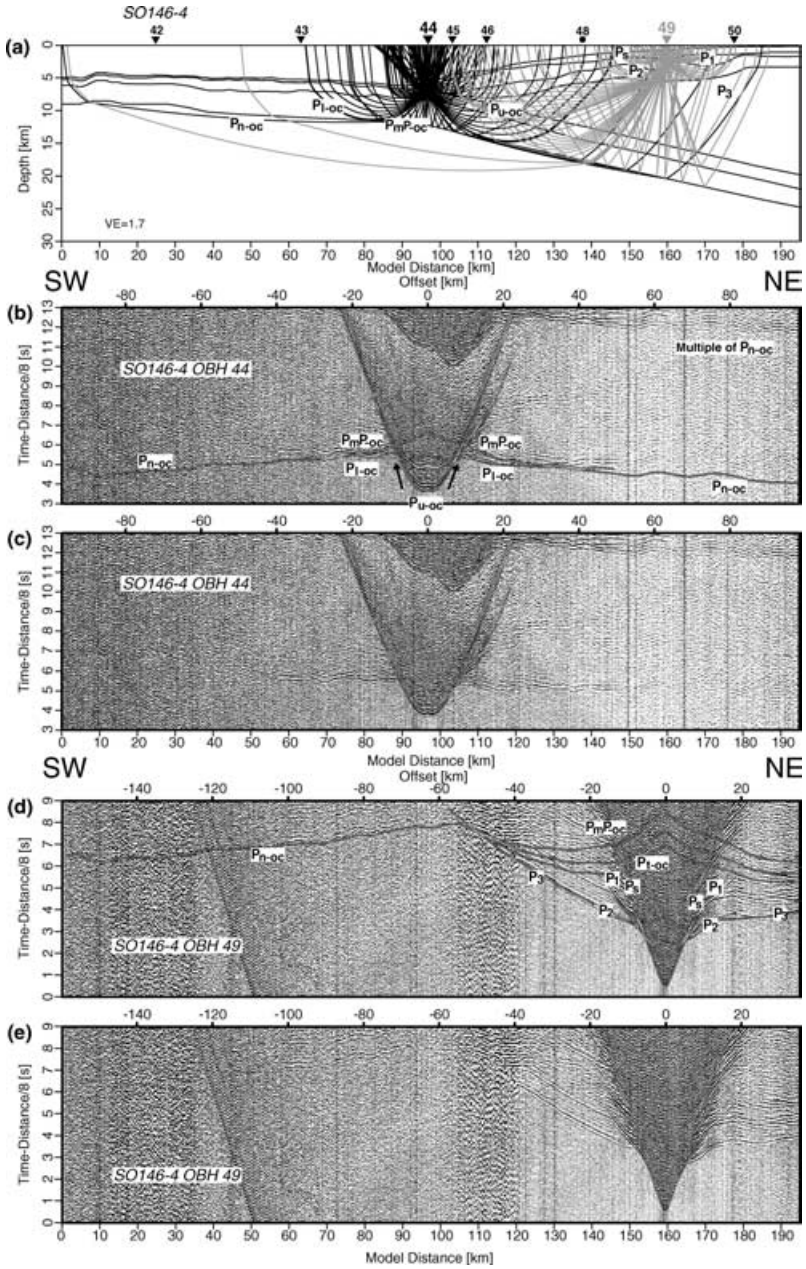

Figure 7. The *P*-velocity model (a) for profile SO146-4/9°S is shown with representative ray paths calculated for the seismic sections below. The record sections OBH 44 and OBH 49 on the oceanic crust/continental margin (c/e) are overlain with traveltime curves (b/d). $P_{t\text{-}oc}$, reflection from top of oceanic crust; $P_{i\text{-}oc}$, intracrustal reflection on the oceanic plate; $P_m P_{\text{-}oc}$, oceanic Moho reflection; $P_{n\text{-}oc}$, oceanic mantle refraction; P_s, refraction from continental sediment; P_1–P_3, refractions from continental interfaces.

Coincident MCS data (line 1018, the landward part published by von Huene & Suess (1988)) constrain the position of the Moho on profile SO146-5/12°S at 2.1 s TWT below the seafloor (von Huene, personal communication). The mean Moho depth is about 6–7 km below the seafloor and the mean *P*-wave velocity of the mantle is about 7.9 km s^{-1}, averaged over the three refraction transects north of the Nazca Ridge.

5.3 The trench

The trench axis is about 6 km deep. There is very little sediment fill visible on all three refraction dip lines, which is consistent with the overall thin sedimentary layer on top of the oceanic Nazca Plate. The trench fill consists of turbidites (Kulm *et al.* 1981). At 0.5 km it is slightly thicker at the northernmost profile SO146-4/9°S than on line SO146-5/12°S, where there is only 0.2 km of trench fill. The trench fill on the southern profile is 0.3 km thick.

The angle of the surface slope with a horizontal line (α), plotted against the dip angle of the subducting plate with the horizontal (β), yields the stability field of a convergent margin (Fig. 14) (Lallemand *et al.* 1994). Their sum is the resulting margin wedge taper ($\gamma = \alpha + \beta$). The surface slope is steep along all three transects with $\alpha = 7.5°$ for SO146-4/9°S, $\alpha = 8.5°$ for SO146-5/12°S and $\alpha = 7°$ for SO146-3/14°S. The dip angle of the subducting plate is $\beta = 7°$ for the northern profile and the two profiles south of the Mendaña Fracture Zone have similar values with $\beta = 5.5°$ for SO146-5/12°S

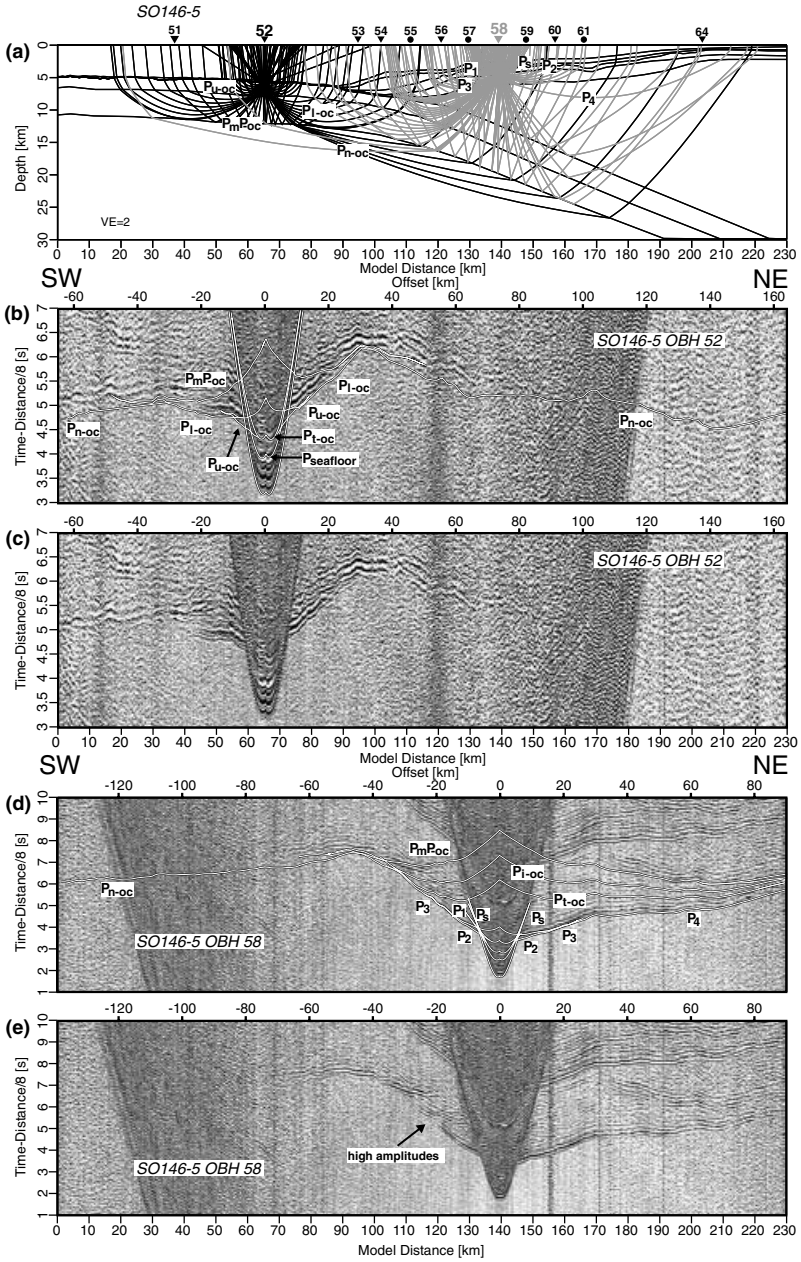

Figure 8. Record sections OBH 52 (a, b and c) and OBH 58 (a, d and e) of profile SO146-5/12°S. See Fig. 7 for details and definitions of abbreviations. The seafloor reflection in record section OBH 52 is not coincident with the direct arrival, because the instrument was placed 600 m above the seafloor.

and $\beta = 6^\circ$ for SO146-3/14°S. The above values result in a taper of $\gamma = 12^\circ$ on profile SO146-3/14°S increasing towards the north with a value of 13° for line SO146-5 and $\gamma = 14.5^\circ$ for the northernmost profile. The taper values were used to compare the Peruvian margin with a global evaluation of the stability field of the margin. The taper derived from all our refraction models is smaller than those for the highly erosive Chilean margin and the Tonga region (Fig. 14, modified after Lallemand *et al.* 1994), but are still consistent with an erosive regime.

5.4 The continental slope and shelf structure

Seismic *P*-wave velocities across the continental slope are characterized by different vertical and lateral gradients. The upper two layers consist of sediments with velocities of 1.6–2.0 km s^{-1} (Fig. 10) and velocities of 2.1–3.3 km s^{-1} increasing from the trench landwards. These are consistent with modelling the traveltimes of the seismic refraction phases P_s and P_1 as denoted in Figs 7–9. The frontal prism is made up of sedimentary deposits added to the toe of the margin, either through accretion (accretionary prism) or due to slope failure (von Huene & Scholl 1991). An increase in the seismic *P*-wave velocity across the frontal prism ($V_p = 2.1$ underneath OBH 54 at profile km 100; Fig. 12) is directly linked to the change in the reflection pattern along the lower slope. Directly seaward and landward of this anomaly, *P*-wave velocities decrease to 1.9–2.0 km s^{-1}. This *P*-wave velocity pattern within the frontal prism can be observed along the three refraction profiles SO146-3/14°S, -4/9°S and -5/12°S.

Yaquina Basin, a 3 km thick forearc basin on the northernmost transect, displays velocities of 1.7–3.0 km s^{-1} (Fig. 10a) within the

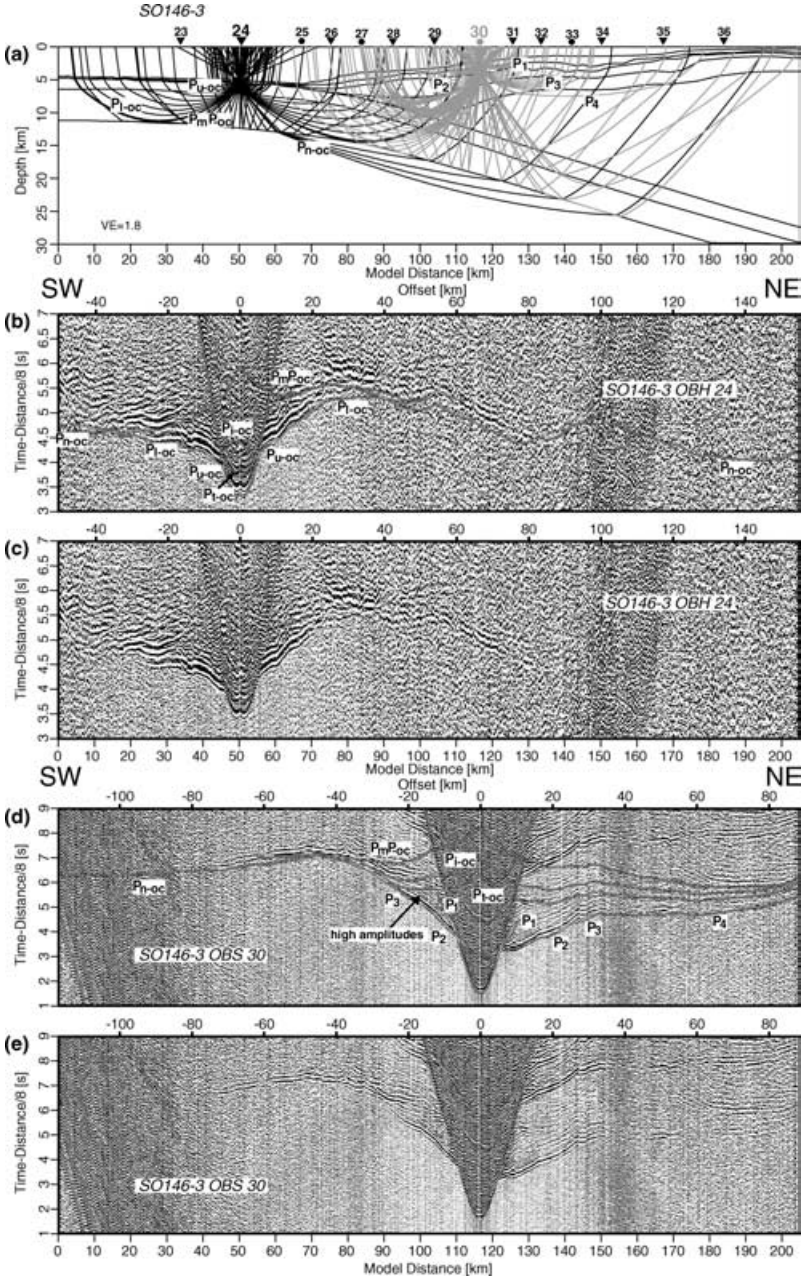

Figure 9. Record sections OBH 24 (a, b and c) and OBS 30 (a, d and e) of profile SO146-3/14°S. See Fig. 7 for details and definitions of abbreviations.

sedimentary fill. Immediately landwards, Trujillo Basin shows the same thickness and seismic *P*-wave velocities. These values correspond to post-Eocene sediments, the uppermost part composed of Neogene slope sediments, which are known from the commercial drill holes Delfin and Ballena (Fig. 2) located on the forearc 80 km further south (Kulm *et al.* 1981). From ODP Leg 112 it is known that the sedimentary sequences in Lima Basin are early Eocene–Quaternary sediments (von Huene & Suess 1988). Along refraction line SO146-5/12°S their thickness is 1.0–1.5 km displaying velocities of 1.7–2.7 km s^{-1}, which agree with the borehole data. Seismic velocities in the West Pisco Basin across the southernmost transect range from 1.6–2.7 km s^{-1} with a total thickness of 2 km. The basins along the northern transect, which were not affected by Nazca Ridge subduction (Hampel 2002), reveal slightly higher seismic velocities and are almost twice as thick as the Lima and West Pisco basins, which in contrast are affected by Nazca Ridge subduction (Hampel 2002). The sedimentary units along the upper slope in the Lima Basin are broken by normal faults (Fig. 4b) indicating extension. The boundary between the second and third layer delimits the top of the crystalline basement, consistent with modelling the traveltimes of the seismic refraction phases P_3 as labelled in Figs 7–9. Our models reveal velocities of 4.5–6.5 km s^{-1} for the continental crust. The latter value is delimited by the ray coverage down to a depth of 25 km. The deepest boundary within the overriding continental plate marks a change in the velocity gradient within the crystalline basement, which is consistent with modelling of the seismic arrivals (designated P_4; Figs 7–9).

The interface between the overriding continental plate and the subducting Nazca Plate is well constrained from the $P_{t\text{-}oc}$ reflection (e.g. Fig. 5). The low *P*-wave velocities across the seaward part

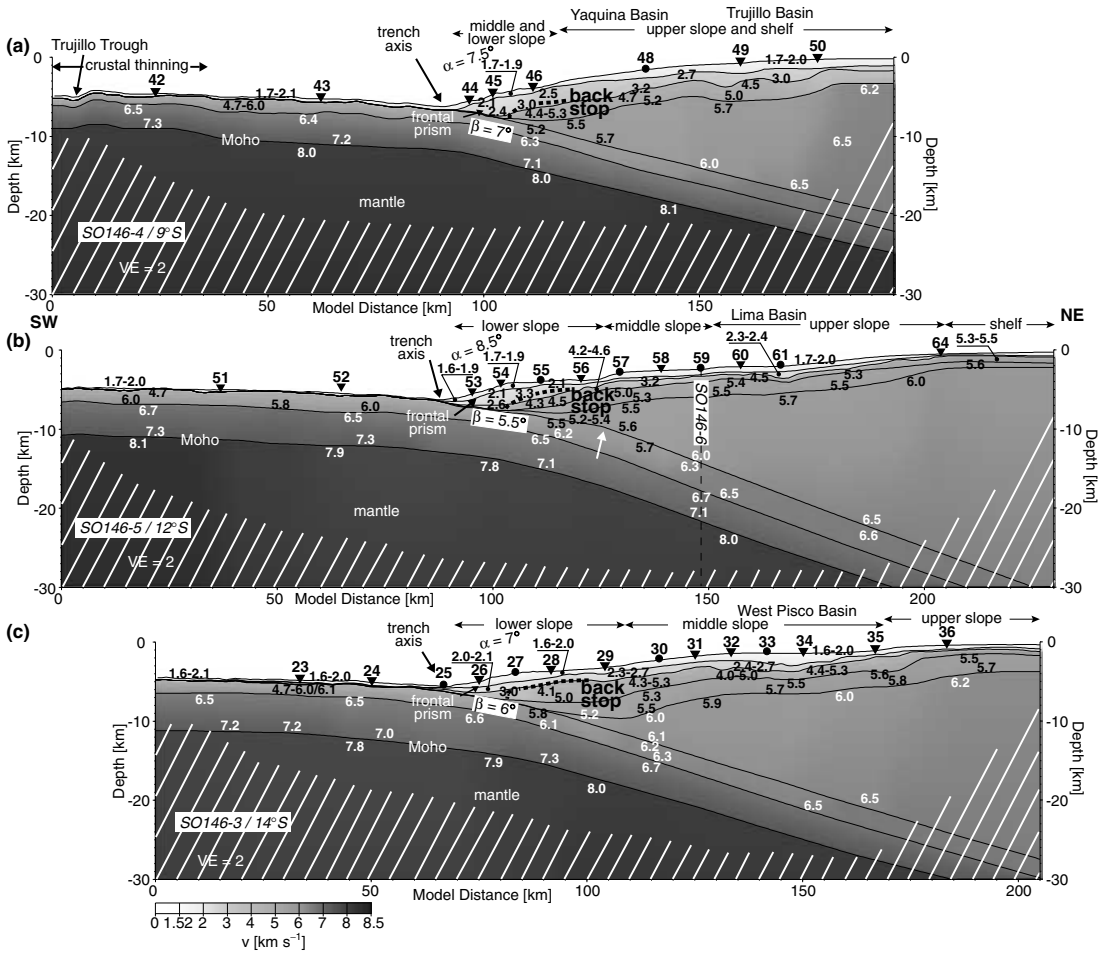

Figure 10. Models obtained from forward modelling of the seismic refraction profiles are displayed from north to south. Note the values of the seismic *P*-wave velocities in the scale below. Locations of the OBH stations are marked by triangles, OBS stations by circles. α and β are the angles of the frontal slope and the dip of the subducting plate, respectively. Only the seawardmost portion of the backstop is marked by a dotted line, it extends further landwards. The white hatched area is not constrained by seismic observations.

of the backstop region (resistive buttress of consolidated sediment and/or rock of the upper plate (von Huene & Scholl 1991); dashed line, Figs 10a–c) infer low seismic velocities on top of the plate boundary within this region. The seismic reflections from the top of the oceanic crust under the backstop region hold high amplitudes, e.g. OBH station 58 and OBS station 30 (Figs 8 and 9). The high amplitudes may originate from a high *P*-wave velocity contrast across the plate boundary indicating the presence of a subduction channel. A subduction channel is present when oceanic sediment remains attached to the subducting oceanic plate and/or material is removed from the upper plate, and which is then subducted (von Huene & Scholl 1991). In addition to the subduction channel, elevated pore fluid pressure, which is likely to be generated by dewatering subducting sediments in that region (Hayward *et al.* 2003; Rüpke *et al.* 2004), may cause the high amplitudes. However, the resolution of the refraction data is not sufficient to resolve a subduction channel of subducting sediment with low seismic *P*-wave velocity at the plate boundary.

The structure of the Lima Basin obtained from the tomographic inversion along the strike-line SO146-6 from 11°S to 12.5°S reveals a 2 km thick upper layer, which is defined by seismic velocities of 1.6–4.5 km s^{-1} (Fig. 11a). The layer below exhibits *P*-wave velocities of 5.0–6.1 km s^{-1}. These are characteristic of the continental crust across the Peruvian margin, which is 8 km thick along profile SO146-6/12°S. The top of the downgoing oceanic plate is at a depth of about 11 km below the seafloor, 60 km landward of the trench axis. The oceanic Moho is displayed in a depth of about 16 km below the seafloor, 60 km landward of the trench axis. The uppermost layer of line SO146-6/12°S is thicker towards the south and the north of the Lima Basin, from 0–40 and 140–170 km. There are also lateral variations in the thickness of the layers below. The thickness decreases towards the peripheral regions, which might be an artefact due to the decreasing resolution of the tomographic inversion (Fig. 11b). Here, we take into account the depth of the ocean–continent boundary along profiles SO146-4/9°S and SO146-3/14°S, 60 km landward of the trench (Figs 10a and c). At this distance, the top of the oceanic plate is located at a depth of 13 km below the seafloor. This provides additional support for the idea that the continental crust may not be thinning towards the peripheral regions of strike-line SO146-6/12°S.

6 DISCUSSION

Our refraction models, obtained by modelling the new seismic refraction data, reveal a 'normal' oceanic crustal composition for the Nazca Plate, covered by a thin pelagic sediment layer (Grevemeyer

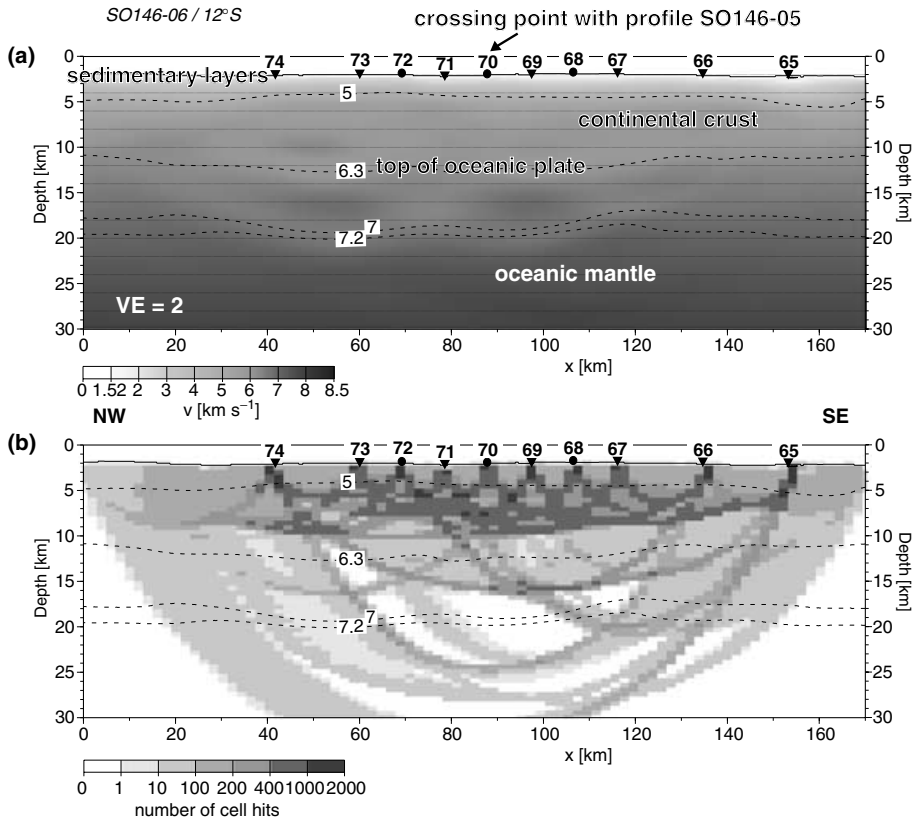

Figure 11. Tomographic inversion of line SO146-6/12°S along the strike of the middle slope of Lima Basin (a). The dashed lines are *P*-wave velocity isolines and the grey-shade code for the velocities can be drawn from the scale. Vertical exaggeration $VE = 2$. (b) The coverage of the seismic tomographic inversion; note the scale below. The resolution is good with some restrictions in the lower corners of the model. Triangles and circles mark OBH and OBS stations, respectively.

et al. 1999; Walther 2003). The thickness of the pelagic sediment layer is variable, sporadically it is lacking, i.e. on profile SO146-5/12°S, where the oceanic crust outcrops, and its maximum thickness is 200 m (Fig. 10). North of the Mendaña Fracture Zone, the Trujillo Trough, a reverse fault, is not just apparent in the high and low structure as revealed by bathymetric measurements, but also to the Moho. The oceanic crust is only 4 km thick in the area of Trujillo Trough compared with an average oceanic crustal thickness of 6.4 km in the study area. The trench turbidites are redeposited from the continental plate due to slope failure. A small amount of trench fill is typical for non-accretive margins (Clift & Vannucchi 2004). The large taper, indicative of high basal friction (Kukowski *et al.* 1994), is further evidence consistent with the Peruvian margin being erosive (Lallemand *et al.* 1994).

The volume of the frontal prism for all profiles is defined by the low seismic velocities of the sediments (Figs 10 and 12), which is consistent with estimates of the frontal prism from earlier interpretations of reflection seismic data (Kulm *et al.* 1981; von Huene & Suess 1988; von Huene *et al.* 1996) and is now verified along the entire Peruvian margin (Figs 10 and 15). The low seismic velocities indicate high porosities and low strength of the frontal prism material that may be explained by overpressured pore fluids in the accreted sediment (Lallemand *et al.* 1994). The frontal prism along the Peruvian margin is small and consistently associated with a steep lower slope. Its width north of the Mendaña Fracture Zone is 15-km. The prism of the central profile (SO146-5/12°S) is of the same size, whereas the frontal prism identified in the southern line extends laterally only to a width of 12 km. It is absent where the Nazca Ridge is currently subducting (Hampel *et al.* 2004). In total, the volumes of the frontal prisms show values of 37 km^3 per trench km for profile SO146-4/9°S, 36.5 km^3 per trench km for profile SO146-5/12°S and 34 km^3 per trench km for profile SO146-3/14°S (Figs 10 and 14). These values were calculated from the pixel information contained in the graphical display of the models (Fig. 15). The conditions across the frontal prism regions of all profiles are similar, i.e. no sediment overburden, similar thickness of frontal prism sediments and similar seismic velocities. Therefore, no further assumptions concerning the porosities of the frontal prism sediments are included in this volume estimate.

These differences in size of the frontal prisms along the Peruvian lower slope may be explained by the influence of the southward-migrating Nazca Ridge on subduction mechanisms. The northern profile has not been affected by the subduction of the Nazca Ridge (Hampel 2002), so it displays a 'normal' stage of subduction at a typical long-term tectonically erosive margin. The two southern profiles display different stages after the Nazca Ridge subduction took place at 11 Ma (the transect across the Lima Basin, SO146-5/12°S) and at 6 Ma (the profile along the West Pisco Basin, SO146-3/14°S) (Hampel 2002). During subduction of the Nazca Ridge, tectonic erosion dominates the subduction processes along the margin (Clift *et al.* 2003), as observed at the present ridge collision zone at 15°S. Six million years after the Nazca Ridge subduction, a small frontal prism has been established at the Peruvian margin at SO146-3/14°S. Eleven million years after Nazca Ridge subduction, the frontal prism imaged at SO146-5/12°S is small in size, typical for an erosional type of margin (i.e. Japan, Tonga region) (von Huene & Scholl 1991;

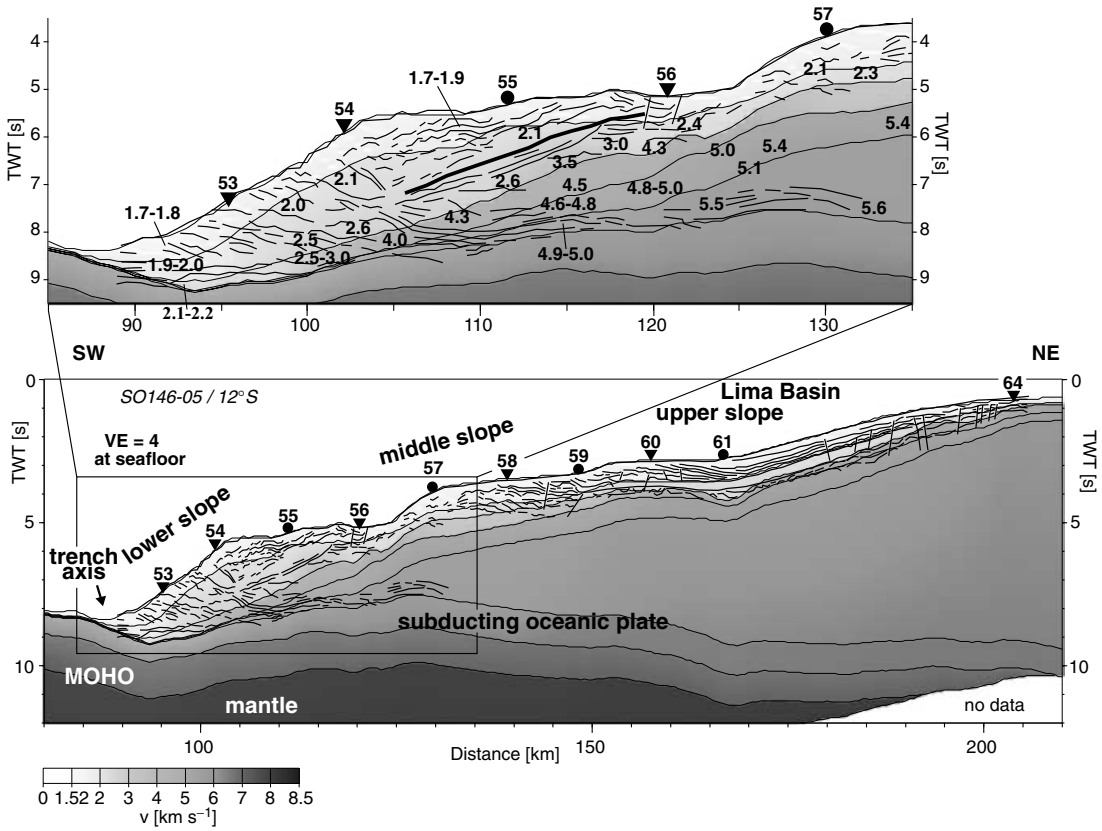

Figure 12. The landward part of the model of profile SO146-5/12°S obtained from forward modelling. It is converted into a time-section and shows good correlation when compared with the line drawing of the coincident seismic record CDP-1 (von Huene & Suess 1988). Locations of the OBH stations are marked by triangles, OBS stations by circles. Seismic *P*-wave velocities are grey-shade coded and annotated at the lower and middle slope.

Collot & Davy 1998), but already completely established, indicating the margin has returned to equilibrium after 11 Myr. This is inferred by a comparison of the width and volume of the frontal prism of profile SO146-4/9°S (both are 15 km wide, with similar volumes (Fig. 15)), which was never affected by the Nazca Ridge subduction. A similar return of the margin to equilibrium has been witnessed also at the Alaska margin in the wake of the Yakutat Block collision (Fruehn *et al.* 1999).

The landward limit of the prism is a backstop structure, which we define by the increasing seismic velocities inferring higher material strength. Increased landward vertical velocity gradients in the refraction models delimit the upper 3 km of the frontal prism. The shape of the backstop derived from the velocity–depth models across the Peruvian margin is between a type I and intermediate backstop structure, as defined by Byrne *et al.* (1993) (Figs 11 and 15). Above the sufficiently strong backstop a bathymetric high has developed, indicating an increase in internal material strength within the margin (Wang & Davis 1996). Numerical and sandbox modelling of the mechanical role of backstops shows that the position of the outer high is located above the toe of the backstop structure (von Huene & Suess 1988; Byrne *et al.* 1993; Wang & Davis 1996). This is consistent with our interpretation in terms of the structure derived from the velocity–depth models. The shape and location of the backstop structure is constrained by the lack of reflection patterns in seismic MCS data as reported by von Huene & Suess (1988) in profile SO146-5/12°S in Fig. 12. From commercial drill holes at 9°S it is known that the continental crust of the Peruvian forearc consists of foliated metamorphic rocks of Palaeozoic or Precambrian age (Kulm *et al.* 1981). However, drilling information is insufficient to define its seaward limit. We define the seaward limit of the continental basement with decreasing seismic velocities (V_p = 3.5–5.0 km s^{-1}). As the Peruvian margin is dominated by long-term erosional processes (von Huene & Suess 1988; von Huene & Scholl 1991; Pecher *et al.* 1996; Clift *et al.* 2003), the seaward part of the backstop may not be an ancient, consolidated accretionary prism but is likely to be composed of (crystalline) continental crust along all three refraction lines. In the region drilled during ODP Leg 112 the Middle Eocene section was drilled along the lower and the middle slope at SO146-5/12°S (von Huene & Suess 1988). Therefore the discrepancy in the seismic velocities (from V_p = 3.5–5 km s^{-1} to V_p = 5–6 km s^{-1}, Figs 10 and 12) infers a difference not in rock composition but in internal structure. This might be due to stronger coupling between the subducting and overriding plates underneath the backstop, resulting in fractures and cracks within the margin wedge material. This complies with high-resolution seismic studies, which indicate fluid migration through fractures and due to anisotropic permeability across the lower slope along the northernmost profile SO146-4/9°S (Hübscher & Kukowski 2003) and the central profile SO146-5/12°S (Pecher *et al.* 2001).

The continental basement causes the overlying sediments to pond against a well-developed outer high in front of a forearc basin (Davis 1996). These form the Yaquina Basin located at the northernmost slope connecting with the upper-slope Trujillo Basin, the Lima Basin across the middle and the West Pisco Basin at the southernmost profile. As described above, the shape of the backstop is similar across the entire Peruvian margin, inferring the same mechanical

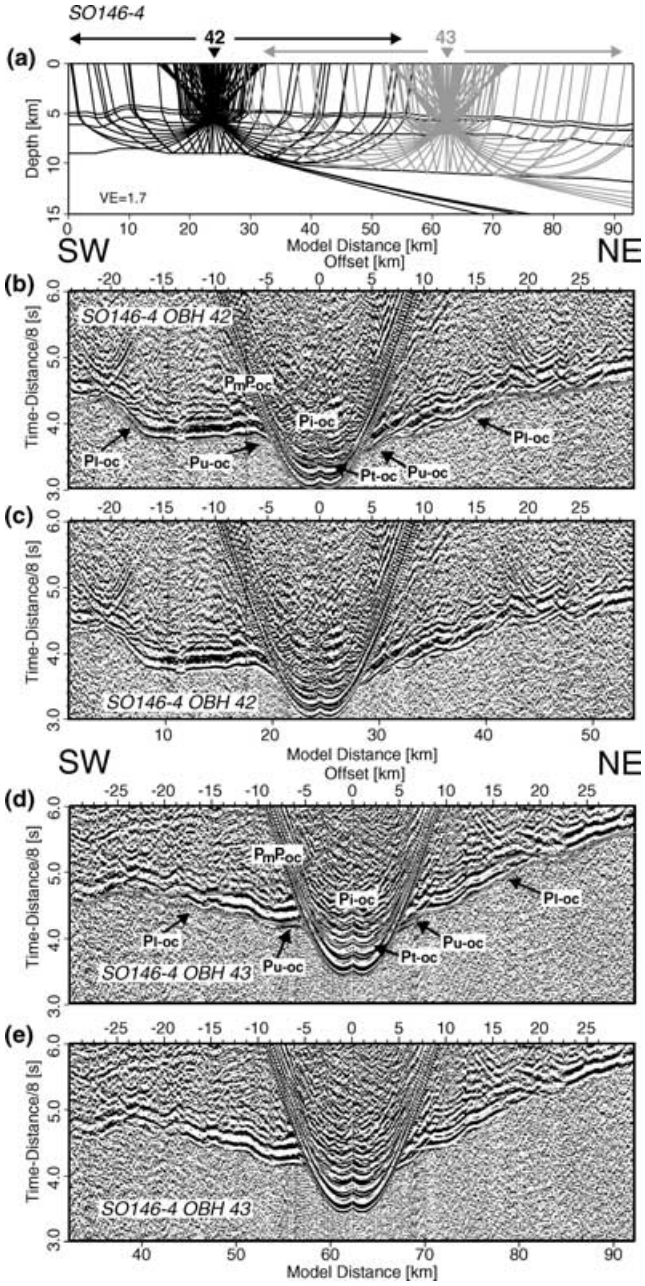

Figure 13. Enlargement of the *P*-velocity model (a) for profile SO146-4/9°S is shown with representative ray paths calculated for the seismic sections below. The regions covered by the enlargements of the seismic sections are marked above the model. Enlargements of record sections OBH 42 and OBH 43 for comparison of the oceanic crustal thickness along the profile (c/e) are overlain with traveltime curves (b/d). See Fig. 7 for details and definitions of abbreviations.

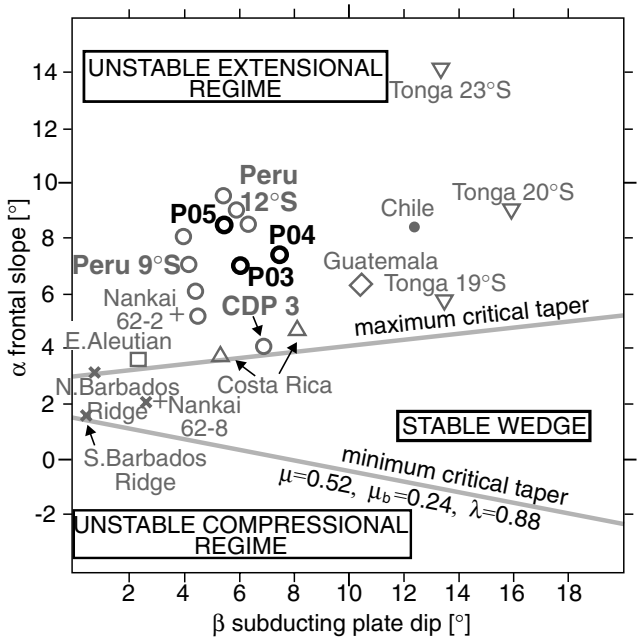

Figure 14. Wedge taper analysis modified after Lallemand *et al.* (1994) with $\mu = 0.52$, $\mu_b = 0.24$ and $\lambda = 0.88$, the values for internal and basal friction and pore fluid pressure ratio, respectively. Three groups of wedges are clearly distinct on this diagram, which are of the accretionary type like Barbados, non-accretionary wedges, i.e. Tonga and northern Chile, and intermediate wedges like Japan and Peru. The wedge tapers, obtained from our refraction models, are designated P03–P05. The subduction angle is largest north of MFZ in the region that is not influenced by the Nazca Ridge subduction.

role for the backstop across the margin. Therefore, the structural difference between the outer highs on the three refraction profiles is explained by differences in the coupling between the subducting and the overriding plate (Davis 1996). The outer high along the transect at SO146-5/12°S is developed due to strong coupling, which produces extremely intense deformation at the toe of the backstop, leading to a high and narrow uplift (Byrne *et al.* 1993). This is constrained by the change in reflection pattern (landward dipping to seafloor parallel) underneath OBH station 54 (Fig. 12). Weaker basal coupling produces a wider outer high, like the topographic structures seen along the slopes of the northern- and southernmost GEOPECO profiles, indicating reduced strength of the backstop.

The sedimentary sequences in the Lima Basin at SO146-5/12°S reveal erosional scarps, which are correlated with the temporary uplift and permanent subsidence at 11 Ma when the Nazca Ridge passed this region (Hampel 2002; Clift *et al.* 2003). The sediment thickness in the basins south of the Mendaña Fracture Zone is 1.5–2.0 km, and therefore about half as thick as the sediments in the Yaquina and Trujillo Basins (SO146-4/9°S), which are around 3 km. This difference is also attributed to the uplift and subsidence caused by the southward migration of the Nazca Ridge and its erosional effect on Peruvian forearc sediments. The slightly higher seismic *P*-wave velocities in the Yaquina and Trujillo Basins, with values from 1.7–3.0 km s^{-1}, compared with the velocities of 1.6–2.7 km s^{-1} in the Lima and West Pisco basins are consistent with the thicker sediments on profile SO146-4/9°S and can therefore be explained by a higher degree of compaction. The rough morphology along the middle slopes of the transects, in addition to the internal material strength, may reflect tectonic activity such as basal removal of upper plate material, which increases the surface slope. This would operate in conjunction with the strong coupling already mentioned above. For line SO146-5/12°S the increase in wedge taper is most distinct at 120 km. Concurrent with the steep slope, indicating high basal friction, we observe steepening of the dip angle of the subducting plate (white arrow, Fig. 10). The observation of increase of the dip angle and consequently the margin wedge taper landward of the trench can now be resolved with the wide-angle seismic data. Previously acquired MCS data were restricted in depth penetration (line drawing, Fig. 12). Therefore we assume that subduction tectonic erosion is most effective in this portion of the plate boundary.

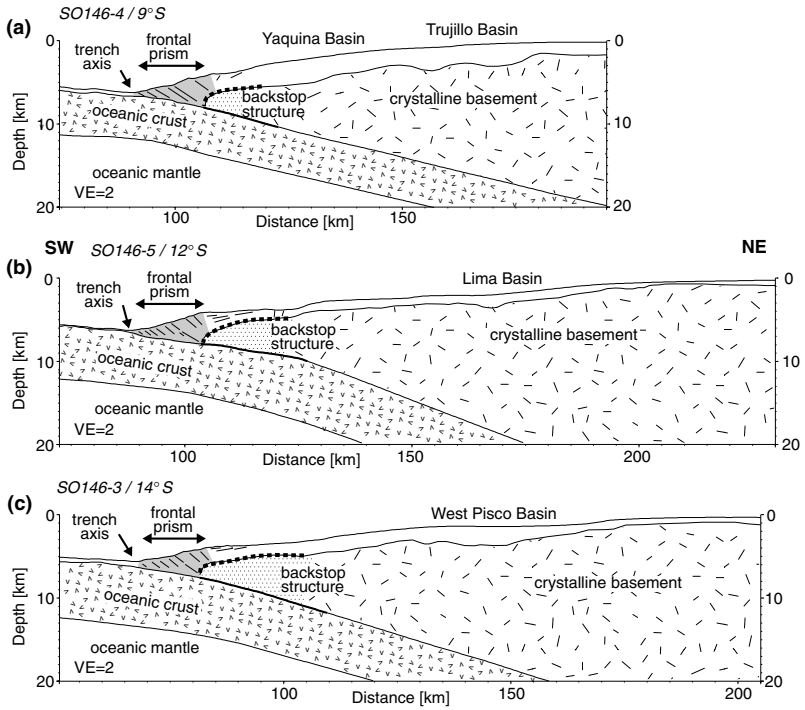

Figure 15. Structural models from north to the south. Line drawings at the toe of the margin are incorporated from earlier reflection seismic studies (Kulm *et al.* 1981; von Huene & Suess 1988). The structure of the backstop has been inferred from *P*-wave velocities derived from the refraction seismic data. The dotted area is characterized by lower seismic velocities than the landward part of the continental crust. The bold line at the continental/oceanic plate boundary marks the zone where we assume that basal erosion is most effective. The grey area for all three profiles contains the pixel information for the calculation of the frontal prism volumes.

This process was described earlier by Adam & Reuther (2000) and von Huene & Ranero (2003) for the Chilean margin.

7 CONCLUSIONS

Seaward of the Peruvian margin, Nazca Plate oceanic crust with a 'normal' velocity structure and topped by a thin pelagic sedimentary layer, varying in thickness from 0–200 m, is approaching the trench. The oceanic crust, with a total thickness of 6.4 km, is divided into an upper and a lower oceanic crustal layer, overlying mantle with a seismic *P*-wave velocity of 7.9 km s^{-1} averaged across the three transects. In the region of the Trujillo Trough at the western part of the northernmost transect, the oceanic crust has a thickness of only around 4 km, probably due to off-axis extension. The plate boundary of the subducting Nazca Plate and the overriding South American Plate is traced down to a depth of 25 km. However, data resolution is not sufficient to resolve a possible subduction channel, although in some areas the presence of subducting sediment is indicated by high amplitudes on top of the subducting oceanic plate. However, the frontal prism and the backstop structure are well defined by their seismic *P*-wave velocities. The same backstop type across the Peruvian margin infers the same mechanical behaviour across the margin wedge. Hence, the different pronounced outer highs (the most distinct being at the middle profile SO146-5/12°S) developed at the toe of the backstop suggest varying material properties within the margin wedge.

Subduction processes along the Peruvian margin are dominated by tectonic erosion, as inferred from the thin sediment fill in the trench, the large taper and the small size of the frontal prism. Tectonic erosion is indicated by the low seismic velocities within the frontal prism, the high convergence rate, the irregular surface slope, the presence of extensional forearc basins, the rough topography of the subducting plate and the retreat of the volcanic front from the Mesozoic to the Late Cenozoic magmatic arc (McKee & Noble 1990). However, frontal tectonic erosion is not the only subduction mechanism across the Peruvian forearc. Basal erosion is most effective where the dip of the subducting plate increases. Basal erosion, as observed here, and related extension leads to the steepening of the trench slope causing slope failure. The failed sediments are transported due to gravitational forces and form the small frontal prism at the toe of the margin. The frontal prisms, missing where Nazca Ridge currently subducts (Hampel *et al.* 2004), and established at the lower slopes 6 Myr and 11 Myr after Nazca Ridge passage, display different evolutionary stages following ridge crest subduction, which is marked by increased erosion. The width of the frontal prism increases from 12 to 15 km, between the profiles from south to the north (SO146-3/14°S and SO146-5/12°S). These 'time slices' indicate, that 11 Myr after collision the margin has returned to equilibrium.

ACKNOWLEDGMENTS

We thank Captain Papenhagen and the crew of R/V *Sonne* for their professional work and support during the GEOPECO cruises. The help of the participants of the GEOPECO cruises with data acquisition and pre-processing is kindly acknowledged. We thank E. R. Flueh for comments on the manuscript. Modelling was performed using MacRay by J. Luetgert and the FAST tomography algorithm was provided by C. Zelt. We used Seismic Unix (Cohen & Stockwell 2001) and GMT (Wessel & Smith 1991) to display the seismic data and for many of the figures. Project SO146 was funded by the German Ministry of Education, Science and Technology Bmbf

(grant no 03G0146A). Careful reviews by P. Clift and K. McIntosh and editorial guidance by J. Francheteau, which helped to improve the manuscript, are kindly acknowledged.

REFERENCES

Adam, J. & Reuther, C.-D., 2000. Crustal dynamics and active fault mechanics during subduction erosion. Application of frictional wedge analysis on to the North Chilean Forearc, *Tectonophysics,* **321,** 297–325.

Bialas, J. & Flueh, E.R., 1999. Ocean bottom seismometers, *Sea Technol.,* **40**(4), 41–46.

Bialas, J. & Kukowski, N. (eds) with contributions from cruise participants, 2000. *FS Sonne Cruise Report So146 1&2 GEOPECO: Geophysical Experiments at the Peruvian Continental Margin, Investigations of Tectonics, Mechanics, Gas Hydrates and Fluid Transport*, GEOMAR, Kiel.

Byrne, D.E., Wang, W-H. & Davis, D.M., 1993. Mechanical role of backstops in the growth of forearcs, *Tectonics,* **12**(1), 123–144.

Clift, P.D. & Vannucchi, P., 2004. Controls on tectonic accretion versus erosion in subduction zones: implications for the origin and recycling of the continental crust, *Rev. Geophys.,* **42,** RG2001, doi:10.1029/2003RG000127.

Clift, P.D., Pecher, I., Kukowski, N. & Hampel, A., 2003. Tectonic erosion of the Peruvian forearc, Lima Basin, by subduction and Nazca Ridge collision, *Tectonics,* **22**(3), 1023, doi:10.1029/2002TC001386.

Cohen, J.K. & Stockwell, J.J.W., 2001. *CWP/SU: Seismic Unix Release 35: a Free Package for Seismic Research and Processing*, Center for Wave Phenomena, Colorado School of Mines.

Collot, J.Y. & Davy, B., 1998. Forearc structures and tectonic regimes at the oblique subduction zone between the Hikurangi Plateau and the southern Kermadec margin, *J. geophys. Res.,* **103**(1), 623–650.

Collot, J.Y., Charvis, P., Gutscher, M.-A. & Operto, S., 2002. Exploring the Ecuador–Colombia active margin and interplate seismogenic zone, *EOS, Trans. Am. geophys. Un.,* **83**(17), 185–190.

Davis, D.M., 1996. Accretionary mechanics with properties that vary in space and time, in *Subduction: Top to Bottom,* AGU Geophysical Monograph Series 96, pp. 39–48, eds Bebout, G.E., Scholl, D.W., Kirby, S.H. & Platt, J.P., American Geophysical Union, Washington, DC.

Flueh, E.R. & Bialas, J., 1996. A digital, high data capacity ocean bottom recorder for seismic investigations, *Int. Underwater Syst. Design,* **18**(3), 18–20.

Fruehn, J., von Huene, R. & Fisher, M.A., 1999. Accretion in the wake of terrane collision: the Neogene accretionary wedge off Kenai Peninsula, Alaska, *Tectonics,* **18**(2), 263–277.

Grevemeyer, I., Kaul, N. & Villinger, H., 1999. Hydrothermal activity and the evolution of the seismic properties of upper oceanic crust, *J. geophys. Res.,* **104**(B3), 5069–5079.

Gutscher, M.-A., Spakman, W., Bijwaard, H. & Engdahl, E.R., 2000. Geodynamics of flat subduction: seismicity and tomographic constraints from the Andean margin, *Tectonics,* **19**(5), 814–833.

Hampel, A., 2002. The migration history of the Nazca Ridge along the Peruvian active margin: a re-evaluation, *Earth planet. Sci. Lett.,* **203,** 665–679.

Hampel, A., Kukowski, N., Bialas, J. & Huebscher, C., 2004. Ridge subduction at an erosive margin: the collision zone of the Nazca Ridge in southern Peru, *J. geophys. Res.,* **109**(2), doi:10.1029/2003JB002593.

Hayward, N., Westbrook, G.K. & Peacock, S., 2003. Seismic velocity, anisotropy, and fluid pressure in the Barbados accretionary wedge from an offset vertical seismic profile with seabed sources, *J. geophys. Res.,* **108**(11), 2515, doi:10.1029/2001JB001638.

Heinbockel, R., Dehghani, G.A. & Huebscher, Ch., 2003. Gravity and magnetic investigations along the Peruvian continental margin, *Geophys. Res. Abstr.,* **5,** 05857.

Hilde, T.W.C. & Warsi, W.E.K., 1982. Subduction induced rifting of the Nazca Plate along Mendana Fracture Zone, *EOS, Trans. Am. geophys. Un.,* **63,** 444.

Hübscher, C. & Kukowski, N., 2003. Complex BSR pattern in the Yaquina Basin off Peru: implications for impact of anisotropic permeability and tectonics, *Geo-Marine Lett.,* **23(2),** 91–101, doi: 10.1007/s00367-003-0128-z.

Huchon, P. & Bourgois, J., 1990. Subduction-induced fragmentation of the Nazca Plate off Peru: Mendana Fracture Zone and Trujillo Trough revisited, *J. geophys. Res.,* **95**(6), 8419–8436.

Hussong, D.M., Dang, S.P., Kulm, L.D. & Couch, R.W., 1984. Jean Charcot Sea Beam survey along ODP leg 112 northern transect, in *Regional Atlas Series, Atlas 9*, 19 Sheets, eds Hilde, T.W.C., Hussong, D.M., Dang, S.P., Kulm, L.D. & Couch, R.W., Ocean Margin Drilling Program, Marine Science International, Woods Hole, MA.

Ito, G., McNutt, M. & Gibson, R., 1995. Crustal structure of the Tuamotu Plateau, 15°S, and implications for its origin, *J. geophys. Res.,* **100**(5), 8097–8114.

Kopp, H. & Kukowski, N., 2003. Backstop geometry and accretionary mechanics of the Sunda margin, *Tectonics,* **22**(6), 1072, doi:10.1029/2002TC001420.

Kukowski, N., von Huene, R., Malavieille, J. & Lallemand, S.E., 1994. Sediment accretion against a buttress beneath the Peruvian continental margin at 12°S as simulated with sandbox modeling, *Geol. Rundschau,* **83,** 822–831.

Kukowski, N., Hampel, A., Bialas, J., Broser, A., Huebscher, C., Barckhausen, U. & Bourgois, J., 2002. Long-term and short-term tectonic erosion at the Peruvian active margin between 9°S and 15°S: evidence from bathymetry data and 3D sandbox analogue modeling, in *5th International Symposium of the Andean Geodynamics*, Toulouse, France, eds Hérail, G. *et al.*, pp. 359–361, Institut de recherche pour le développement, Paris, France.

Kulm, L.D., Prince, R.A., French, W., Johnson, S. & Masias, A., 1981. Crustal structure and tectonics of the central Peru continental margin and trench, *Geol Soc. Am. Mem.,* **154,** 445–468.

Lallemand, S.E., Schnürle, P. & Malavieille, J., 1994. Coulomb theory applied to accretionary and nonaccretionary wedges: possible causes for tectonic erosion and/or frontal accretion, *J. geophys. Res.,* **99**(6), 12 033–12 055.

Luetgert, J., 1992. MacRay-Interactive two-dimensional seismic raytracing for the Macintosh, *US Geological Survey Open File Report,* 92–356.

McKee, E.H. & Noble, D.C., 1990. Cenozoic tectonic events, magmatic pulses, and base- and precious metal mineralization in the central Andes, in *Geology of the Andes and its Relation to Hydrocarbon and Mineral Resources*, Earth Science Series, Vol. 11, pp. 189–194, eds Ericksen, G.E., Pinochet, M.-T.C. & Reinemund, J.A. Circum-Pacific Council for Energy & Mineral Resources, Texas.

Moore, G.F. & Taylor, B., 1988. Structure of the Peru forearc from multichannel seismic reflection data, in *Proc. ODP, Initial Reports,* Vol. 112, pp. 71–76, ed. Stewart, S.K., Ocean Drilling Program, College Station, TX.

Müller, R.D., Roest, W.R., Royer, J.-Y., Gahagan, L.M. & Sclater, J.G., 1997. Digital isochrons of the world's ocean floor, *J. geophys. Res.,* **102,** 3211–3214.

Norabuena, E.O., Snoke, J.A. & James, D.E., 1994. Structure of the subducting Nazca Plate beneath Peru, *J. geophys. Res.,* **99**(5), 9215–9226.

Norabuena, E.O., Dixon, T.H., Stein, S. & Harrison, C.G.A., 1999. Decelerating Nazca–South America and Nazca–Pacific Plate Motions, *Geophys. Res. Lett.,* **26**(22), 3405–3408.

Parsons, B. & Sclater, J.G., 1977. An analysis of the variation of ocean floor bathymetry and heat flow with age, *J. geophys. Res.,* **82**(5), 803–827.

Pecher, I.A., Minshull, T.A., Singh, S.C. & von Huene, R., 1996. Velocity structure of a bottom simulating reflector offshore Peru: results from full waveform inversion, *Earth planet. Sci. Lett.,* **139,** 459–469.

Pecher, I.A., Kukowski, N., Hübscher, C., Greinert, J. & Bialas, J., 2001. The link between bottom-simulating reflections and methane flux into the gas hydrate stability zone; new evidence from Lima Basin, Peru margin, *Earth planet. Sci. Lett.,* **185,** 343–354.

Pilger, R.H., Jr, 1981. Plate reconstructions, aseismic ridges, and low-angle subduction beneath the Andes, *Geol. Soc. Am. Bull., Pt I,* **92,** 448–456.

Pilger, R.H., Jr. & Handschumacher, D.W., 1981. The fixed-hotspot hypothesis and origin of the Easter-Sala y Gomez-Nazca trace, *Geol. Soc. Am. Bull., Pt I,* **92,** 437–446.

Protti, M., Güendel, F. & McNally, K., 1995. Correlation between the age of the subducting Cocos Plate and the geometry of the Wadati–Benioff zone under Nicaragua and Costa Rica, in *Geologic and Tectonic Development of the Caribbean Plate Boundary in Southern Central America,* GSA Special Paper 295, pp. 309–326, ed. Mann, P. Geological Society of America, Boulder, CO.

Purdy, G.M., Kong, L.S.L., Christeson, G.L. & Solomon, S.C., 1992. Relationship between spreading rate and seismic structure of mid-ocean ridges, *Nature,* **355,** 815–817.

Rüpke, L.H., Phipps Morgan, J., Hort, M. & Connolly, J.A.D., 2004. Serpentine and the subduction zone water cycle, *Earth planet. Sci. Lett.,* **223,** 17–34, doi:10.1016/j.epsl.2004.04.018.

Sandwell, D.T. & Smith, W.H.F., 1997. Marine gravity anomaly from Geosat and ERS1 satellite altimetry, *J. geophys. Res.,* **102,** 10 039–10 054.

Vogt, P.R., Lowrie, A., Bracey, D.R. & Hey, R.N., 1976. *Subduction of Aseismic Oceanic Ridges: Effects on Shape, Seismicity and other Characteristics of Consuming Plate Boundaries*, GSA Special Paper 172, p. 59, Geological Society of America, Boulder, CO.

von Huene, R. & Ranero, C.R., 2003. Subduction erosion and basal friction along the sediment-starved convergent margin off Antofagasta, Chile, *J. geophys. Res.,* **108,** doi:10.1029/2001JB001569.

von Huene, R. & Scholl, D.W., 1991. Observations at convergent margins concerning sediment subduction, subduction erosion, and the growth of continental crust, *Rev. Geophys.,* **29**(3), 279–316.

von Huene, R. & Suess, E., 1988. Ocean Drilling Program Leg 112, Peru continental margin: part 1, tectonic history, *Geology,* **16,** 934–938.

von Huene, R., Pecher, I.A. & Gutscher, M.-A., 1996. Development of the accretionary prism along Peru and material flux after subduction of Nazca Ridge, *Tectonics,* **15**(1), 19–33.

Walther, C.H.E., 2003. The crustal structure of the Cocos ridge off Costa Rica, *J. geophys. Res.,* **101**(5), 2136, doi:10.1029/2001JB000888.

Wang, W-H. & Davis, D.M., 1996. Sandbox model simulation of forearc evolution and noncritical wedges, *J. geophys. Res.,* **108**(B3), 11 329–11 339.

Wessel, P. & Smith, W.H.F., 1991. Free software helps map and display data, *EOS, Trans. Am. geophys. Un.,* **72,** 441,445–446.

Zelt, C.A., 1999. Modelling strategies and model assessment for wide-angle seismic traveltime data, *Geophys. J. Int.,* **139,** 183–204.

Zelt, C.A. & Barton, P.J., 1998. Three dimensional seismic refraction tomography: a comparison of two methods applied to data from the Faeroe Basin, *J. geophys. Res.,* **103**(4), 7187–7210.